Sampled-Data Modeling for PCM and ZVS Controlled Critical Conduction Mode (CrCM) Active Clamp Flyback (ACF) Converter at Variable Switching Frequency

Shengyou Xu, Qinsong Qian, Ran Shi, Syed Sikandar Shah, Qi Liu, Shengli Lu, and Weifeng Sun, *Senior Member, IEEE*

***Abstract*— Critical conduction mode (CrCM) active clamp flyback (ACF) converter is regarded as a good candidate for low power adaptor applications. However, the most adopted control strategy of variable-frequency peak current mode (VF-PCM) and discrete zero voltage switch (ZVS) control makes it difficult to get the accurate small signal model. Therefore, by using sampled-data modeling method, this paper proposes an exact small signal model of CrCM ACF converter for the first time. In the modeling process, the influence of discrete-ZVS control is firstly considered. The conduction time of power switch is regarded as the control signal, which is different from constant-frequency converter. The total current close-loop transfer function is simplified by the linear combination of single VF-PCM and discrete-ZVS control model. After considering the sampling effect and the modulator gain from the derived sampled-data model respectively, the control-to-output transfer function of CrCM ACF converter is developed. The analytical results are analyzed by comparing with single VF-PCM and the widely used average model. Finally, to validate the accuracy of the proposed model, a 65W 20V output CrCM ACF converter is simulated and measured. The verification shown that the proposed sampled-data model is basically agreement with the simulation and experimental results.**

***Index Terms*— Sampled-data model, Active clamp flyback (ACF) converter, Critical conduction mode (CrCM), Peak Current mode (PCM), Zero voltage switch (ZVS), Variable-frequency.**

I. Introduction

With the rapid development of portable electronic products, the people's demands on size and charging time reduction of mobile adapters are becoming higher and higher, which further result in the increasing requirements of power density and efficiency. It is an effective way to improve the power density of power supplies by increasing frequency, but which decreases the efficiency of hard switching converters such as the widely used RCD clamp flyback converter [1]–[3]. Therefore, it is very beneficial to replace the current hard switching converter by adopting soft switching topology.

Compared with flyback converter, Active clamp flyback (ACF) utilize a clamp capacitor and a clamp power switch [4]–[6] to replace the RCD clamp circuit. Hence, the leakage inductor energy is absorbed by clamp capacitor, part of this energy is applied to realize ZVS for primary power switch, and the other part is transferred to secondary. Although in some operation status or high frequency, the leakage inductor energy is insufficient to achieve ZVS, ACF still can be designed to operate in critical conduction mode (CrCM) to use the magnetizing inductor energy to help realize ZVS [7]. Therefore, CrCM ACF converter can switch very efficiently and realize ZVS easily at full load range by controlling the magnetizing current. Otherwise, with proper design and control, output rectifier diode can achieve zero current switch off (ZCS) during turn-off, thus the rectifier snubber is not needed. Overall, CrCM ACF converter is a good candidate to be utilized in high-frequency high-efficiency power supplies, to satisfy the requirements of small size and high power density. The circuit topology of ACF converter is shown in Fig.1.

It is very suitable to utilize variable frequency peak current mode (VF-PCM) and ZVS combination control method for a high-performance and good-dynamic CrCM ACF converter [8], [9]. In this methodology, ZVS control is adopted to regulate the switching period for an appropriate negative magnetizing current, and then to realize the ZVS of primary power switch. Therefore, CrCM ACF should be operated in variable frequency. The switching period is only updated at the start time of every switching cycle makes CrCM ACF has a discrete period renew process, so the ZVS control can be called "discrete-ZVS control", which will be mentioned later. The same as constant-frequency PCM (CF-PCM) controlled converter [10], the VF-PCM control method in CrCM ACF converter is used to adjust the conduction time of power switch for a good dynamic. The detailed control process will be illustrated in the following section.

Small signal model has popularly used for the dynamic performance and frequency analysis of many DC-DC converters [11]–[17], such as buck [18]–[20], boost [10], [21]–[23],

Manuscript received October 7, 2019; revised February 7, 2020 and March 30, 2020; accepted April 26, 2020. This work was supported in part by the Natural Science Foundation of Jiangsu Province under Grant BK20171155 and in part by the Key Research and Development Plan of Jiangsu under Grant BE2018003-3. This article was recommended by Associate Editor K.-H. Chen. *(Corresponding author: Weifeng Sun.)*

The authors are with the National ASIC System Engineering and Research Center, Southeast University, Nanjing 210096, China (e-mail: swffrog@seu.edu.cn).

Color versions of one or more of the figures in this article are available online at http://ieeexplore.ieee.org.

Digital Object Identifier 10.1109/TCSI.2020.2993256

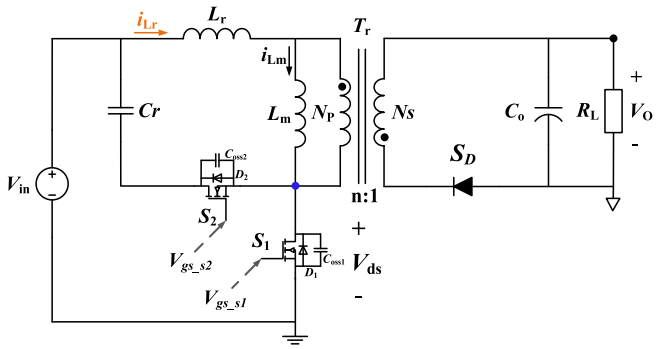

Fig. 1. The circuit topology of ACF converter.

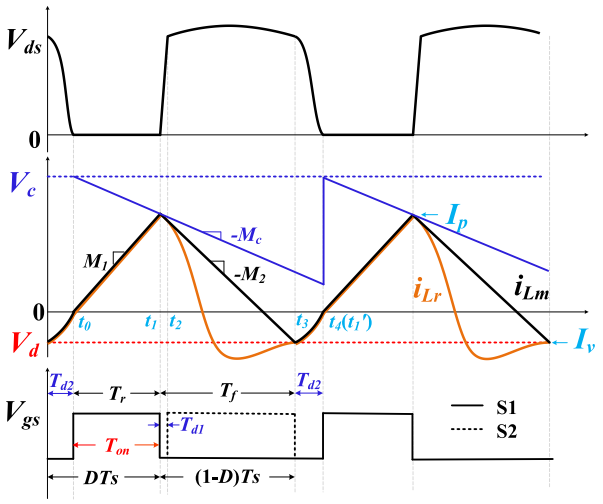

Fig. 2. Steady-state waveforms of CrCM ACF converter.

buck-boost [24]–[26], and SEPIC [27] converter. However, due to the distinctive and complicated control strategy, the accurate small signal mode of VF-PCM and discrete-ZVS controlled CrCM ACF converter has not been published yet. Unlike constant-frequency converter [11]–[27], the conduction time of power switch and switching period vary synchronously in every switching cycle in variable-frequency converter. Thus, the widely used control variable, duty ratio, cannot by regarded as the single control signal in VF-PCM controlled converter. In other words, duty ratio cannot be directly used to derive the small signal model of VF-PCM controlled CrCM ACF converter. Moreover, the discrete-ZVS control principle also makes it is difficult to get the accurate small signal model which can also reflect the frequency characteristic of ZVS control process.

To solve the modeling problem in variable-frequency converter, replaced duty ratio by the on-time constraint of power switch, Suntio [28] extended average model into BCM flyback converter. Then Park *et.al* [29] gave the PWM switch model of CrCM converter by applied Suntio's modeling method in the same year. Afterwards, Ayachit derived the circuit average model for BCM boost converter [30]. However, it is well known that the average model is only accurate up to the half of switching frequency in constant-frequency converter. Therefore, it also has the same shortcoming of Suntio's method if it is used in CrCM or BCM converter. Besides this faultiness, average model cannot be well used to illustrate the frequency characteristic of ZVS controlled CrCM ACF converter owing to the discrete-ZVS control rule. Sampled-data model is another important modelling method, and which can predict the well-known subharmonic oscillation, hence it is widely used in CF-PCM controlled converters [31]. However, in variable-frequency converter, in addition to Pagano [32] had given the sampled-data model for hysteresis current mode (HCM) controlled converter, to forecast the bifurcation phenomena between CCM and DCM, there are no more papers illustrated. In his modeling process, based on state space averaging (SSA) method, the operation time is also treated as a variable, rather than a sampling point in the sampled-data model of CF-PCM controlled converter [31]. Thus the innate character of his modeling method still based on average model. Since the modeling object is dual-mode controller, and switching period is constant in every cycle if operating conditions are determined, the modeling method proposed by Cheng [33] cannot be used to model the VF-PCM and discrete-ZVS controlled CrCM ACF converter. Otherwise, his modeling process is too complicated to be used for the small signal model of HCM or BCM converter.

Therefore, based on the proposed control methodology, to derive an accurate small signal model of CrCM ACF converter, the VF-PCM and discrete-ZVS control process are all considered by using sampled-data modeling method. In addition, the control signal, duty ratio, is replaced by the conduction time of power switch in the modeling process. This work is organized as follows.

The operation process, the VF-PCM and discrete-ZVS combination control strategy of CrCM ACF converter are introduced in details in Section II. In section III, the current close-loop model of CrCM ACF converter is simplified by the linear combination of single VF-PCM and discrete-ZVS control model. Therefore, the current close-loop transfer function is obtained after the single VF-PCM and discrete-ZVS model is derived by sampled-data modeling method respectively. In Section IV, the control-to-output transfer function of CrCM ACF converter is developed by considering the sampling effect and the modulator gain of the two control models, respectively. Then the frequency characteristic of the proposed model is analyzed by comparing with single VF-PCM, Suntio's average model, and equivalent circuit model. In section V, the SIMPLIS simulation results are presented to verify the accuracy of the proposed sampled-data model. Moreover, a VF-PCM and discrete-ZVS controlled CrCM ACF prototype is designed and tested, the experimental results are given. The conclusion is summarized in Section VI.

II. VF-PCM and Discrete-ZVS Control Strategy

Fig.2 shows the waveforms of CrCM ACF converter. i_{Lr} and i_{Lm} are the resonant and magnetizing current, respectively. V_{gs} is the gate signal of primary power switch S_1 and S_2, V_{ds} is the voltage between the drain and source of the primary main power switch S_1. Based on these waveforms, the operation process of CrCM ACF converter can be classified as four main operating modes from $t = t_0$ to $t = t_4$.

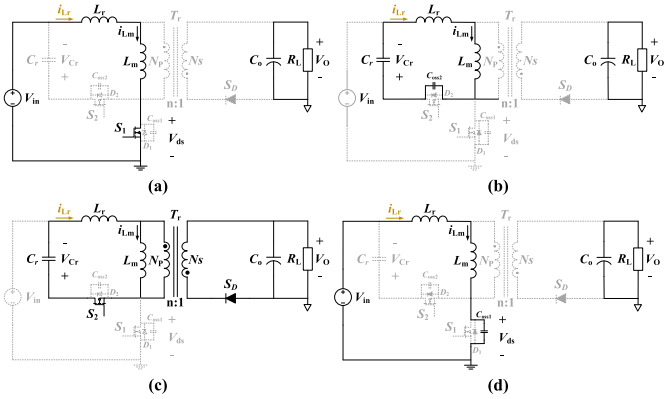

Fig. 3. The main equivalent circuits of CrCM ACF converter.

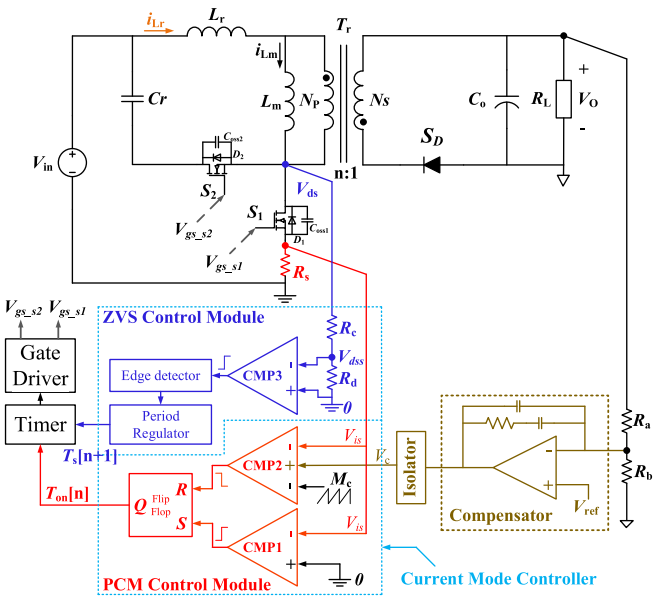

Fig. 4. The circuit topology and corresponding control diagram of CrCM ACF converter.

The first one is energy storage mode from $t = t_0$ to $t = t_1$. The energy stored in magnetizing inductor L_m and leakage inductor L_r are charged by input source V_{in}, so i_{Lr} and i_{Lm} are increased linearly. Since the energy cannot be transferred from primary to secondary, the output voltage V_o is stabled by output capacitor C_o.

The second one is the first ZVS realization mode for the clamp power switch S_2 in T_{d1} from $t = t_1$ to $t = t_2$. During this mode, L_m and L_r are resonant with the parasitic capacitance C_{oss} of S_2, and then the voltage between the drain and source of S_2 is discharged by i_{Lr} and i_{Lm}. Thus, the ZVS of S_2 can be realized if the body diode of S_2 start to flow current.

The third one is energy transfer mode from $t = t_2$ to $t = t_3$. Due to the energy can be delivered from primary to secondary, L_m is clamped by V_o. L_r is resonant with the clamp capacitor C_r, so i_{Lr} and i_{Lm} are varied sinusoidally and linearly, respectively.

The fourth one is the second ZVS realization mode for S_1 in T_{d2} from $t = t_3$ to $t = t_4$. In this mode, because of L_m is not clamped by the output voltage V_o, so which is also join into the resonant process with L_r and the parasitic capacitance C_{oss} of S_1. V_{ds} is discharged by i_{Lm}, so the ZVS of S_1 can be reached if V_{ds} is decreased to zero.

The equivalent circuit of the four modes are shown in Fig.3 (a)-(d), respectively. The detailed operation processes can be referred in [4]–[6].

VF-PCM and discrete-ZVS control method is very suitable to be used for a high performance CrCM ACF converter. The VF-PCM and discrete ZVS control diagram is shown in Fig.4. As the figure shown, current mode control is used to obtain high performance, and which include a voltage loop and a current loop. In the voltage loop, the output voltage V_o is sensed by a resistance network consisting of two resistors R_a and R_b, then through a compensator and an isolator to generate compensated voltage V_c. In the current loop, there are two control modules. The one uses PCM control to regulate the conduction time T_{on} of S_1 to stable the output voltage, and the other one applies ZVS control to adjust the switching period T_s to get high-efficiency.

According to the waveforms shown in Fig.2, for a high-efficiency, the start time of the main power switch S_1 should be set at the zero-crossing point of the magnetizing current i_{Lm}. Therefore, in the PCM control module, the comparator CMP1 is used to compare the sensed magnetizing current signal V_{is} which is generated through a sampling resistance R_s, and zero, then to determine the start time of S_1. S_1 is turned on if i_{Lm} is reached to zero. For a high dynamic characteristic, the same as the PCM control in [10], the comparator CMP2 is applied to compare the compensated voltage V_c, the sensed current signal V_{is}, and the slope compensation M_c, and then to determine the end-time of S_1. S_1 is switched off if i_{Lm} is reached to V_c minus the relative compensated slope value. Therefore, the conduction time of S_1 can be performed in every switching cycle if the start time and end time of S_1 are determined in the PCM module. Afterwards, the clamp power switch S_2 is conducted complementarily with S_1. The start time S_2 arrives after the dead time T_{d1} is finished. The conduction time of S_2 equals to the switching period T_s minus the two dead times, T_{d1} and T_{d2}. Where, T_{d1} and T_{d2} are two constants, and which are used to realize the ZVS of S_2 and S_1, respectively.

At the turn-off moment of S_1, the magnetizing current i_{Lm} is locating at its peak I_p, so just a small dead time T_{d1} is needed for the ZVS realization of S_2. In other words, the ZVS of S_2 can be easily realized cause of its needed energy is sufficient in T_{d1}. However, i_{Lm} is nearby its valley I_v during the turn-off instant of S_2, the energy used to realize the ZVS of S_1 maybe not enough in T_{d2}. Hence, the ZVS of S_1 may not be realized in T_{d2} at some operation status, such as in low input voltage and high load current conditions. Therefore, for a high-efficiency CrCM ACF converter, the magnetizing current valley I_v should be regulated to ensure the ZVS of S_1 can be achieved no matter what conditions. It is an effective way to adjust I_v by changing the switching period T_s in every switching cycle. The larger T_s is, the larger conduction time of S_2 is, and the larger I_v is generated to ensure that ZVS

of S_1 can be achieved. However, redundant I_v will result in additional power loss, so T_s should be controlled precisely.

In the ZVS control module, the comparator CMP3 is applied to compare V_{ds} and zero to estimate the ZVS status at the turn-on instant of S_1. The edge detector is used to check the output signal variation of CMP3, and then to regulate the switching period T_s of the next switching cycle. If V_{ds} is smaller than zero, indicates that ZVS of S_1 has been realized, then the next switching period T_s[n+1] will be decreased by the period regulator. On the contrary, T_s[n+1] will be increased. To clearly express the adjustment law of T_s, and convenient for the following sampled-data modeling, a ZVS control signal V_d is used in Fig.2 to illustrate the control strategy of T_s in CrCM ACF converter. In an established operation status, regulate T_s to generate proper I_v value, equals to the turn-off moment of S_2 is determined by the suitable ZVS control signal V_d. Therefore, V_d can be represented by I_v in (1). Note that, the same to the refresh time of T_s, which is at the start time of every cycle, the update instant of V_d also is set at this moment.

$$V_d = R_s I_v \tag{1}$$

Accordingly, based on the PCM and ZVS control modules, the conduction time T_{on} and switching period T_s can be regulated for a high dynamic high-efficiency CrCM ACF converter. Owing to T_{on} and T_s vary in every switching cycle, the duty ratio cannot be regarded as the single control signal in variable-frequency PCM (VF-PCM) controlled CrCM ACF converter. Otherwise, due to the switching period T_s only update at the start time of S_1, the regulation law of switching period is discrete, so the ZVS control can be called "discrete-ZVS control".

By using energy transfer principle, the input power can be calculated by (2). Through averaging and approximating the current waveform of S_1, the average input current I_{in} is expressed in (3). Otherwise, based on the triangular waveform of i_{Lm}, duty ratio D, the decrease time T_f, and the switching period T_s can be easily expressed by (4), (5) and (6), respectively.

$$P_{\text{in}} = V_{\text{in}} I_{in} = \frac{V_o I_o}{\eta} \tag{2}$$

$$I_{in} = \frac{I_v T_{d2} + I_p T_r}{2T_s} \tag{3}$$

$$D = \frac{T_r + T_{d2}}{T_r + T_{d2} + T_f} \tag{4}$$

$$T_f = \frac{(I_p - I_v) L_m}{n V_o} \tag{5}$$

$$T_s = T_r + T_f + T_{d2} \tag{6}$$

where, V_{in} and V_o are the input and output voltage, respectively. I_o is the full load current. η is the presumptive operation efficiency. n is the ratio between primary and secondary winding of ACF transformer. L_m is the magnetizing inductor. T_r is the conduction time of S_1. I_p is the peak current of i_{Lm}. I_v is the minimum negative current of i_{Lm}.

Associate with (1) - (6), the relationship between T_s and other system parameters can be deduced by (7). This expression represents the change regulation of T_s at different line and load status, to regulate T_s at different turn ratio n, magnetizing inductor L_m, and output voltage V_o, and then to obtain an optimal working efficiency η. This equation also gives the relationship between T_s and V_d, which will be used in the modeling process.

$$T_s = \frac{(1-D) R_s V_{in} V_o n\eta + 2 R_s V_o I_o L_m - D V_{in} L_m \eta V_d}{D(1-D) R_s V_{in} V_o n\eta} \tag{7}$$

III. Sampled-Data Model of Current Close-Loop

According to mentioned above, in order to obtain high efficiency in high frequency applications, CrCM ACF converter should be operated at variable-frequency, the conduction time T_{on} of S_1 and switching period T_s should be changed to regulate output voltage V_o and ZVS status. Therefore, duty ratio D can't be regarded as the single control signal to model the variable-frequency CrCM ACF converter. Although replaced duty ratio D by conduction time T_{on}, average modeling method can be used in variable-frequency converter, the accuracy is limited at half of the switching frequency, and the small signal influence of the discrete ZVS control process can't be contained. By considering the switching status in every cycle, sampled-data model remains much high-frequency information [31], but which hasn't been well applied in variable-frequency CrCM converter due to duty ratio D and switching period T_s changed synchronously in every regulating cycle. To solve this problem, replace duty ratio D by the discrete conduction time T_{on}[n] of S_1, an accurate sampled-data model of VF-PCM and discrete-ZVS controlled CrCM ACF converter at variable-frequency is established in this paper.

Fig.5 shown the steady state and perturbed magnetizing current waveforms of CrCM ACF converter. To express it clearly, there are two points have been simplified. Firstly, the current waveforms in T_{d2} are replaced by using a straight line, but they are still regarded as resonant form in calculating process. The slope of the straight line is approximated as M_1 [34]. Secondly, the resonant current i_{Lr} and the gate signal of S_2 are concealed to avoid visual confusion.

As shown in Fig.5, the steady state and perturbed waveforms are expressed by solid and dotted line, respectively. T_{on} and T'_{on} are the steady state and perturbed conduction time of S_1, respectively. T_s and T'_s are the steady state and perturbed switching period, respectively. From this figure, it can be clearly seen that T_{on} and T_s are changed when a small signal perturbation is added on the magnetizing current i_{Lm}. By using simple parallelogram law, the conduction time perturbation $\hat{T}_{on}$ can be obtained by (8).

$$\hat{T}_{on} = T'_{on} - T_{on} = D' T'_s - D T_s \tag{8}$$

where, D and D' are the steady state and perturbed duty ratio, respectively. Add perturbation on D' and T'_s, namely $D' = D + \hat{d}$, $T'_s = T_s + \hat{T}_s$. Then (8) can be transferred to

$$\hat{T}_{on} = (D + \hat{d})(T_s + \hat{T}_s) - D T_s = T_s \hat{d} + D \hat{T}_s + \hat{d} \hat{T}_s \tag{9}$$

Neglect high-frequency nonlinear small signal terms, the small signal linear relation among $\hat{T}_{on}$, $\hat{d}$ and $\hat{T}_s$ is given

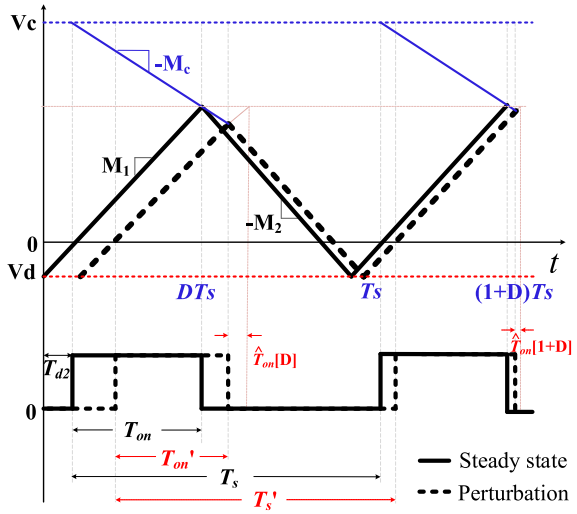

Fig. 5. The steady state and perturbed magnetizing current waveforms of CrCM ACF converter.

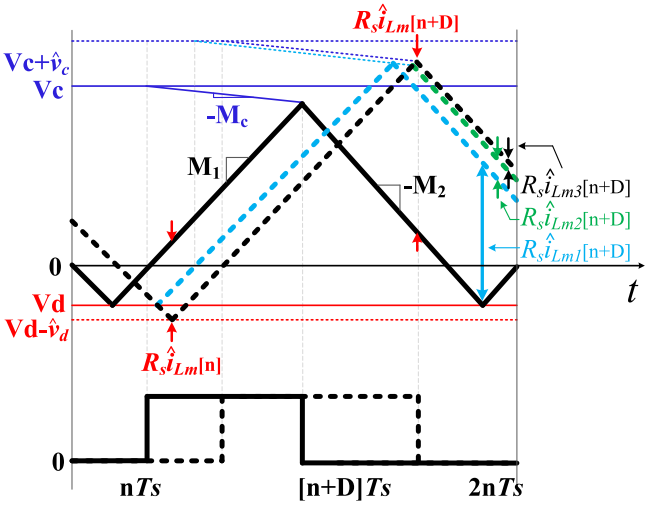

Fig. 6. The perturbed waveforms of CrCM ACF converter.

in (10). According to (7), the perturbation relationship between $\hat{d}$ and $\hat{T}_s$ can be got in (11).

$$\hat{T}_{on} = T_s\hat{d} + D\hat{T}_s \tag{10}$$

$$H_{dt} = \frac{\hat{d}}{\hat{T}_s} = \frac{D(1-D)nV_oR_s}{nV_oR_s(1+(2D-1)T_s) + L_mV_d} \tag{11}$$

Substituting (11) into (10), equations (12) and (13) can be derived. Through these two equations, the conduction time perturbation $\hat{T}_{on}$ can be transformed into the control signal $\hat{d}$ or $\hat{T}_s$ directly and easily. These two equations are much beneficial to the needed control signal transformation, and (12) will be used in the following discrete-ZVS control modeling process.

$$\hat{T}_{on} = (T_sH_{dt} + D)\hat{T}_s \tag{12}$$

$$\hat{T}_{on} = (T_s + \frac{D}{H_{dt}})\hat{d} \tag{13}$$

A. Model Simplification

From Fig.5, it also can be seen that the VF-PCM control signal V_c and discrete-ZVS control signal V_d jointly determine the operation status of CrCM ACF converter. Therefore, to derive an accurate sampled-data model, both of the influence of VF-PCM and discrete-ZVS control need be considered.

Fig.6 shows the perturbed waveforms of CrCM ACF converter. The black solid line is the steady state waveforms, the black dotted line is the perturbed waveforms when the perturbation $\hat{v}_c$ and $\hat{v}_d$ are occurred synchronously. The blue and green dotted lines are applied for auxiliary analysis. Relative to steady state, the blue dotted line is the perturbed waveform when the perturbation $\hat{v}_c$ only been happened. Compare with the blue dotted line, the green dotted line is the perturbed waveform when only considering the perturbation $\hat{v}_d$. According to the distribution of the magnetizing current perturbation $R_s\hat{\dot{i}}_{Lm}$ at time [n+D]T_s, the total perturbation $R_s\hat{\dot{i}}_{Lm}[n+D]$ included three parts, namely

$$R_s\hat{i}_{Lm}[n+D] = R_s\hat{i}_{Lm1}[n+D] + R_s\hat{i}_{Lm2}[n+D] + R_s\hat{i}_{Lm3}[n+D] \tag{14}$$

where, R_s is the current sampling resistance. $R_s\hat{\dot{i}}_{Lm1}$ [n+D] represents the perturbation when $\hat{v}_c$ is only considered. $R_s\hat{\dot{i}}_{Lm2}$ [n+D] represents the perturbation when $\hat{v}_d$ is only considered. $R_s\hat{\dot{i}}_{Lm3}$ [n+D] is the synthetic action of the two perturbation signals, which represents $\hat{v}_c$ is formed passively since $\hat{v}_d$ is considered. Through simple analysis, $R_s\hat{\dot{i}}_{Lm3}$ [n+D] can be approximately substituted by $R_s\hat{\dot{i}}_{Lm2}$ [n+D] with a scale factor.

$$R_s\hat{i}_{Lm3}[n+D] \approx \frac{m_c(m_1+m_2)}{m_1m_2}R_s\hat{i}_{Lm2}[n+D] \tag{15}$$

where, m_1 and m_2 are the rising and falling slope of the magnetizing current, respectively. m_c is the external compensated slope. Substituting (15) into (14), the total magnetizing current perturbation $R_s\hat{\dot{i}}_{Lm}[n+D]$ at time [n+D]T_s can be calculated by the linear combination of $R_s\hat{\dot{i}}_{Lm1}$ [n+D] and $R_s\hat{\dot{i}}_{Lm2}$ [n+D].

$$R_s\hat{i}_{Lm}[n+D] = R_s\hat{i}_{Lm1}[n+D] + K_mR_s\hat{i}_{Lm2}[n+D] \tag{16a}$$

where,

$$K_m = 1 + \frac{m_c(m_1+m_2)}{m_1m_2} \tag{16b}$$

According to (16), the control-to-current transfer function can be derived by the linear combination of the two terms [35]. Because of $R_s\hat{\dot{i}}_{Lm1}$ [n+D] represents the small signal influence of the single VF-PCM control, $R_s\hat{\dot{i}}_{Lm2}$ [n+D] represents the small signal influence of the single discrete-ZVS control, the current close-loop modeling process can be simplified by the two single control strategy. Therefore, the total current close-loop model can be separated into single VF-PCM control and discrete-ZVS control model.

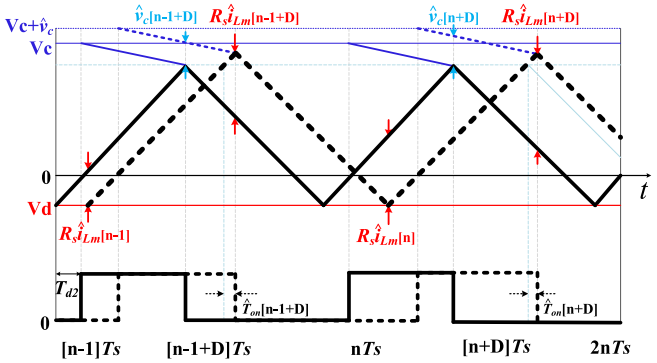

Fig. 7. The perturbed VF-PCM control signal waveforms.

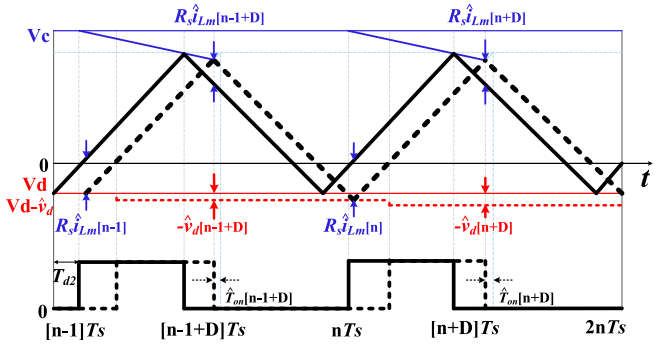

Fig. 8. The perturbed ZVS control signal waveforms.

B. Single VF-PCM Control Model

The sampled-data modeling method has widely used in the PCM controlled converter [29], [32], [33], but which are mainly in constant-frequency converter. Fig.7 shows the perturbed waveforms to derive the single VF-PCM control model in CrCM ACF converter. As the figure shown, the conduction time perturbation $\hat{T}_{on}$, the switching period perturbation $\hat{T}_s$ and the magnetizing current perturbation $R_s\hat{i}_{Lm}$ are produced result from the PCM control signal perturbation $\hat{v}_c$.

By adding auxiliary line, using parallelogram law and similar triangle rule, based on the conduction time perturbation $\hat{T}_{on}$ of S_1, the following difference equations can be obtained.

$$R_s\hat{i}_{Lm}[n+D]=R_s\hat{i}_{Lm}[n-1+D]+(m_1+m_2)\hat{T}_{on}[n+D] \tag{17}$$

$$\hat{v}_c[n+D]=\frac{m_c}{m_2}R_s\hat{i}_{Lm}[n-1+D]+(m_1+m_c)\hat{T}_{on}[n+D] \tag{18}$$

These two equations show the small signal perturbation relationship between magnetizing current $\hat{i}_{Lm}$, PCM control signal $\hat{v}_c$ and conduction time $\hat{T}_{on}$ in VF-PCM control. Due to the different intermediate control variable, the two equations are different to the difference equation in CF-PCM control [35]. Through combining these two equations, and using z-transformation, the transfer function of VF-PCM control model in z-domain is given as

$$H_p(z)=\frac{R_s\hat{i}_{Lm}(z)}{\hat{v}_c(z)}=\frac{\alpha_{pb}}{1-(1-\alpha_{pa})z^{-1}} \tag{19a}$$

where,

$$\alpha_{pb}=\frac{m_2-m_c}{m_1+m_c} \tag{19b}$$

$$\alpha_{pa}=\frac{m_c}{m_2}\alpha_{pb} \tag{19c}$$

By using the transfer equation from s-domain to z-domain $z=e^{sT_s}$, and multiplying by the sample and hold function $\frac{1-e^{sT_s}}{sT_s}$. Then the VF-PCM control transfer function in s-domain can be derived in (20).

$$H_p(s)=\frac{R_s\hat{i}_{Lm}(s)}{\hat{v}_c(s)}=\frac{\alpha_{pb}}{1-(1-\alpha_{pa})e^{-sT_s}}\frac{1-e^{-sT_s}}{sT_s} \tag{20}$$

Use Padé approximation

$$z=e^{sT_s}\approx\frac{1+\frac{sT_s}{2}+\frac{(sT_s)^2}{12}}{1-\frac{sT_s}{2}+\frac{(sT_s)^2}{12}}=\frac{s^2+6f_s s+12f_s^2}{s^2-6f_s s+12f_s^2} \tag{21}$$

The simple style close-loop transfer function of VF-PCM control can be easily obtained.

$$H_p(s)=\frac{R_s\hat{i}_{Lm}(s)}{\hat{v}_c(s)}=\frac{12\alpha_{pb}f_s^2}{\alpha_{pa}s^2+(12-6\alpha_{pa})f_s s+12\alpha_{pa}f_s^2} \tag{22}$$

C. Discrete-ZVS Control Model

Fig.8 shows the perturbed ZVS control signal waveforms in CrCM ACF converter. According to the control strategy of discrete-ZVS control, every refresh time of T_s is at the turn-on instant of S_1. Therefore, in order to derive an accurate small signal model, the control signal V_d also need updating at this moment. Hence, a discrete perturbation $-\hat{v}_d$ is added on V_d to imitate the regulation strategy of T_s, which is only changed at the turn-on moment of S_1, and kept constant in a whole switching cycle.

The conduction time T_{on}, the switching period T_s and the magnetizing current $R_s i_{Lm}$ change with the ZVS control signal V_d. The same to VF-PCM control model, by using parallelogram law and trigonometric approximation, the difference equation of discrete-ZVS control can be derived.

$$\begin{aligned}R_s\hat{i}_{Lm}[n+D]=&R_s\hat{i}_{Lm}[n-1+D]-\frac{m_1+m_2}{m_1}\hat{v}_d[n-1+D]\\&-(m_1+m_2)\hat{T}_{on}[n+D]\end{aligned} \tag{23}$$

Equation (23) shows the relationship among the conduction time perturbation $\hat{T}_{on}$, the magnetizing current perturbation $R_s\hat{i}_{Lm}$, the ZVS control signal perturbation $\hat{v}_d$. Because of the discrete renewal law of $\hat{v}_d$ in every switching cycle, there is only one difference equation in ZVS control. Therefore, to deduce the control-to-current transfer function, the perturbation relationship between $\hat{T}_{on}$ and $\hat{v}_d$ need to be derived firstly. According to (7), the perturbation relation between $\hat{T}_s$ and $\hat{v}_d$ can be obtained.

$$H_{tv}=\frac{\hat{T}_s}{\hat{v}_d}=-\frac{L_m}{R_s(1-D)nV_o} \tag{24}$$

Combine (24) and (12), the perturbation relationship between $\hat{T}_{on}$ and $\hat{v}_d$ is given as.

$$\hat{T}_{on} = (T_s H_{dt} + D) H_{tv} \hat{v}_d \tag{25}$$

Substituting (25) into (23), the difference equation of discrete ZVS control model can be deduced in (26). Note that $\hat{T}_{on}[n+D]$ is affected by $\hat{v}_d[n-1+D]$, not by $\hat{v}_d[n+D]$.

$$R_s \hat{i}_{Lm}[n+D] = R_s \hat{i}_{Lm}[n-1+D] + \beta_v \hat{v}_d[n-1+D] \tag{26a}$$

where,

$$\beta_v = -\frac{m_1 + m_2}{m_1} - (m_1 + m_2)(T_s H_{dt} + D) H_{tv} \tag{26b}$$

The same operation is processed in VF-PCM control model. Through z-transform, considering the sample and hold effect, the transfer function of discrete ZVS control model is derived in (27). Use Padé approximation, the approximate s-domain transfer function of discrete ZVS control model is given in (28).

$$H_v(s) = \frac{R_s \hat{i}_{Lm}(s)}{\hat{v}_d(s)} = \frac{\beta_v e^{-sT_s}}{sT_s} \tag{27}$$

$$H_v(s) = \frac{R_s \hat{i}_{Lm}(s)}{\hat{v}_d(s)} = \frac{\beta_v f_s (s^2 - 6 f_s s + 12 f_s^2)}{s(s^2 + 6 f_s s + 12 f_s^2)} \tag{28}$$

D. Total Current Close-Loop Transfer Function $G_{ic}(s)$

According to Fig.6 and (16), the total current close-loop transfer function is the linear combination of the VF-PCM and discrete-ZVS control model transfer function. Therefore, after substituting (22) and (28) into (16), the full-order current close-loop transfer function can be derived in (29).

$$G_{ic}(s) = \frac{K_{i4}s^4 + K_{i3}s^3 + K_{i2}s^2 + K_{i1}s + K_{i0}}{s(s^2 + 6 f_s s + 12 f_s^2)(\alpha_{pa} s^2 + (12 - 6\alpha_{pa}) f_s s + 12 \alpha_{pa} f_s^2)} \tag{29a}$$

where,

$$K_{i0} = 144 f_s^5 \alpha_{pa} \beta_v K_m \tag{29b}$$

$$K_{i1} = -144 f_s^4 ((\alpha_{pa} - 1)\beta_v K_m - \alpha_{pb}) \tag{29c}$$

$$K_{i2} = 12 f_s^3 ((5\alpha_{pa} - 6)\beta_v K_m + 6\alpha_{pb}) \tag{29d}$$

$$K_{i3} = -12 f_s^2 ((\alpha_{pa} - 1)\beta_v K_m - \alpha_{pb}) \tag{29e}$$

$$K_{i4} = f_s \alpha_{pa} \beta_v K_m \tag{29f}$$

IV. Small Signal Model of VF-PCM and Discrete-ZVS Controlled CrCM ACF Converter

A. Control-to-Output Transfer Function $G_{vc}(s)$

The small signal modeling strategy of the VF-PCM and discrete ZVS controlled CrCM ACF converter is shown in Fig.9. The corresponding control-to-output transfer function $G_{vc}(s)$ is defined as $v_{out}(s)/v_{c\_total}(s)$. Where, $v_{c\_total}(s)$ is an assumed total control signal and which has considered the combined influence of VF-PCM and discrete ZVS control effect. From this figure, it can be seen that the total model

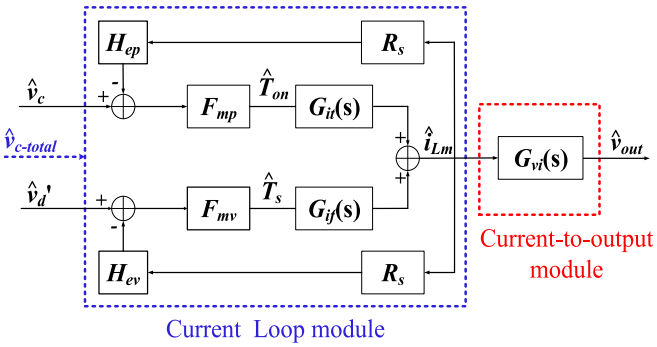

Fig. 9. Modeling strategy of CrCM ACF converter.

includes two modules, current loop module, and current-to-output module. Therefore, the control-to-output transfer function $G_{vc}(s)$ can be derived by multiplying the two parts.

In the current control loop module, VF-PCM control signal $\hat{v}_c$ and discrete ZVS control signal $\hat{v}_d'$ are the input signals; magnetizing current $\hat{i}_{Lm}$ is the output signal. Base on (16), $\hat{v}_d'$ represents the proportion K_m has been considered. $G_{it}(s)$ is the conduction time to magnetizing current transfer function in VF-PCM control model. $G_{if}(s)$ is the switching period to magnetizing current transfer function in discrete ZVS control model. These two transfer functions can be deduced by the variable-frequency average modeling method introduced in [28].

R_s is the gain of magnetizing current sensor. As the simplified control circuit shown in Fig.4, circuit delay are usually existed in the applied sampling circuit of VF-PCM and ZVS control module, so which may have a big influence on the finally modeling result. Therefore, these problems need to be considered in the control-to-output transfer function derivation process. In Fig.9, H_{ep} and H_{ev} are the used sampling gain to illustrate the circuit detection delay of VF-PCM and discrete-ZVS control module, respectively. They are can be represented by the sampling transfer function in (30) [36].

$$H_e(s) = \frac{s \cdot T}{e^{s \cdot T} - 1} \tag{30}$$

which has a pair of double poles at the half of switching frequency. Generally, based on the sampling theory, it only considers the frequency zone [0, f_s/2]. Then, the two-order approximation of (30) is given as

$$H_e(s) \approx \frac{s^2}{w_n^2} + \frac{s}{w_n \cdot Q_z} + 1 \tag{31a}$$

Where

$$w_n = \pi \cdot f_s \tag{31b}$$

$$Q_z = -\frac{2}{\pi} \tag{31c}$$

Similarly, the used comparators in VF-PCM and discrete ZVS control module are nonlinear components [37]. Therefore, the regulating ability also need to be considered if the small signal model is derived. In Fig.9, F_{mp} and F_{mv} are the modulator gain of VF-PCM and discrete ZVS control module respectively, which represent the ability to regulate the

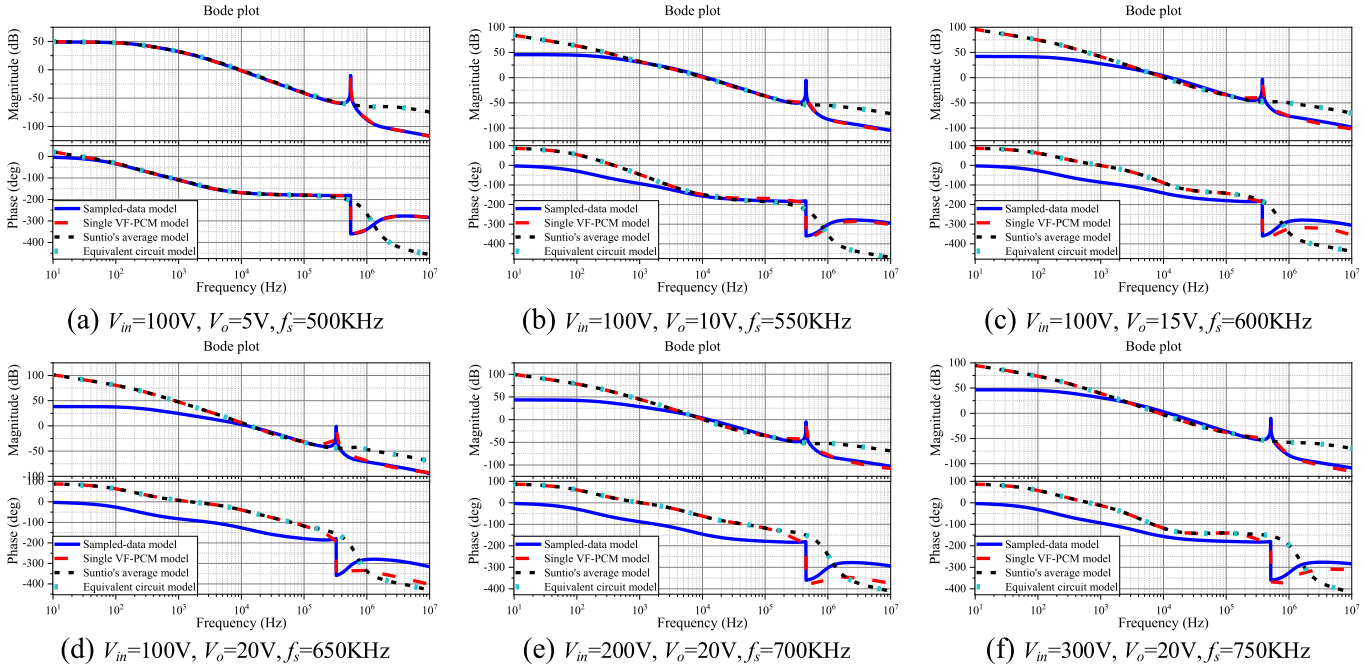

(a) V_{in}=100V, V_o=5V, f_s=500KHz (b) V_{in}=100V, V_o=10V, f_s=550KHz (c) V_{in}=100V, V_o=15V, f_s=600KHz

(d) V_{in}=100V, V_o=20V, f_s=650KHz (e) V_{in}=200V, V_o=20V, f_s=700KHz (f) V_{in}=300V, V_o=20V, f_s=750KHz

Fig. 10. Frequency response comparison at different operating status.

conduction time T_{on} and switching period T_s in VF-PCM and discrete ZVS control model, respectively. To fully taking the comparator errors into considered, by using the similar method in [31], F_{mp} and F_{mv} can be deduced by (32) and (33).

$$F_{mp} = \frac{H_p(s)}{(R_s H_{ev} H_v(s) - 1)G_{it}(s)} \tag{32}$$

$$F_{mv} = \frac{H_v(s)}{(R_s H_{ev} H_v(s) - 1)G_{if}(s)} \tag{33}$$

The current-to-output module transfer function $G_{vi}(s)$, defined as $\hat{v}_{out}(s)/\hat{i}_{Lm}(s)$. Although the average model ignores many high frequency signals result from the averaged and linearized process, it's enough to modeling the current-to-output transfer function. Therefore, followed by the average modeling method of CrCM converter introduced in [28], the magnetizing current-to-output transfer function $G_{vi}(s)$ is given as (34).

$$G_{vi}(s) = \frac{L_m[(DL_mL_rC_r)s^3+(L_mD(1-D)^2)s-R_Ln^2(1-D)^4]}{n(1-D)[(L_mL_rC_rC_oR_L)s^3+(L_mL_rC_rn^2(1+D))s^2 +(1-D)^2R_L(n^2C_r(L_m+L_r)+L_mC_o)s-L_m(1+D)(1-D)^2]} \tag{34}$$

Consequently, according to the small signal model framework in Fig.9, the control-to-output transfer function $G_{vc}(s)$ is given as

$$G_{vc}(s) = \frac{R_sF_{mp}G_{it}(s)G_{vi}(s)}{1+R_sH_{ep}F_{mp}G_{it}(s)} + \frac{R_sF_{mv}G_{if}(s)G_{vi}(s)}{1+R_sH_{ev}F_{mv}G_{if}(s)} \tag{35}$$

B. Frequency Response Curve Comparison

By utilizing MATLAB software, the frequency response curves of the control-to-output transfer function $G_{vc}(s)$ at different operating conditions are shown in Fig.10. In order to validate the modeling effect of the proposed sampled-data model of VF-PCM and discrete-ZVS controlled CrCM ACF converter, the single VF-PCM control model which not contain ZVS control effect, the Suntio's model [28] which uses averaging algorithm, and Park's equivalent circuit model [29] are also provided.

In Fig.10 (a)-(c), the input voltage is fixed at 100V, but the output voltage change from 5V to 15V with a step 5V. In Fig.10 (d)-(f), the output voltage is stabled at 20V, but the input voltage increase from 100V to 300V with a step 100V. In all the operating status, to regulate the ZVS realization, the switching frequency should be changed, so which is assumed increasing from 500KHz to 750KHz with a step 50KHz, respectively. Note that, the switching period is not just increased by input voltage, which is determined by input voltage and load current synchronously. This will be illustrated later.

Due to the same modeling principle, the frequency response curves of the equivalent circuit model and Suntio's average model are agreement with each other. By comparing the proposed sampled-data model with single VF-PCM and average model, it can be seen that, in most cases, when the discrete-ZVS control strategy is used to realize ZVS status and improve operating efficiency, the control-to-output frequency response curves are changed. The reason is that the regulating principle of CrCM ACF converter has varied since the discrete-ZVS control process is utilized to regulate the switching period. For instance, when load current increases, the output voltage start decreasing, the conduction time of primary main power switch S_1 will be improved by the VF-PCM control to make the output voltage return. On the other hand, a smaller negative magnetizing current valley I_v (or a positive I_v) is produced since the increased load current,

TABLE I
SIMULATION PARAMETERS

Symbol	Parameter name	Quantity
V_{in}	Input voltage	100V-380V
V_{out}	Output voltage	20V
P_{out}	Output power	65W
f_s	Switching frequency	600K-1MHz
L_m	Magnetizing inductor	32uH
L_r	Resonant inductor	1.8uH
C_r	Clamp capacitor	50nF
C_o	Output Capacitor	200uF

so a larger switching period will be generated by the discrete ZVS control to stable I_v at the original value. However, the increased switching period results in a decreased output voltage, which is contrary to the improved conduction time of S_1. Therefore, the regulating process of the proposed control method is different to PCM control, and there are a different frequency characteristic between them. Accordingly, the accuracy of single VF-PCM and average model are suspected when the ZVS control strategy is adopted, and the control characteristic and dynamic performance will be affected if the questioned model is used in control loop design.

By comparing the average model with single VF-PCM model, due to the averaged and linearized modeling process, the high frequency information is ignored, average model just can fit well with the single VF-PCM control model in low and middle frequency band, even though the conduction time also has been regarded as the control signal.

V. SIMULATION AND EXPERIMENTAL VERIFICATION

A. SIMPlis Simulation Comparison

SIMPLIS simulation software is accurately and popularly utilized in many small signal model verifications [33], [35]. Therefore, in order to verify the proposed sampled-data model, SIMPLIS simulation software is used and a VF-PCM and discrete-ZVS controlled CrCM ACF converter is simulated. The simulated parameters of CrCM ACF converter are shown in table I.

The comparison results between the proposed model and SIMPLIS simulation at three different operating conditions are shown in Fig.11-13, respectively. It is explicitly shown here that the proposed model is basically consistent with the SIMPLIS simulation results. Although there is small difference in the middle frequency band between the proposed model and SIMPLIS simulation results, the proposed model still can be used for control loop analysis and compensator design due to the influence of discrete ZVS control is considered. Therefore, the proposed sampled-data model is more accurate than the single VF-PCM and average model if the VF-PCM and discrete-ZVS control strategy is adopted in CrCM ACF converter.

B. Experimental Results

To further verify the proposed sampled-data model, a 65W 19.5V output digital VF-PCM and discrete-ZVS controlled

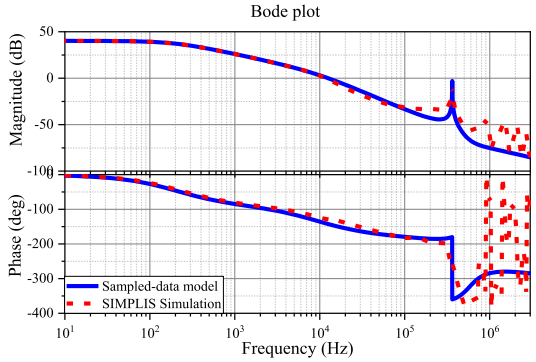

Fig. 11. SIMPLIS simulation verification G_{vc} when V_{in} =120V, V_o =20V, 100% load.

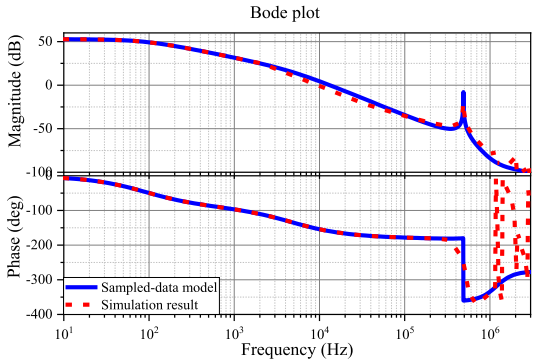

Fig. 12. SIMPLIS simulation verification G_{vc} when V_{in} =250V, V_o =20V, 50% load.

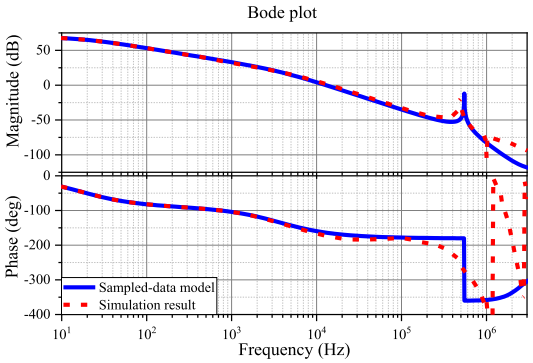

Fig. 13. SIMPLIS simulation verification G_{vc} when V_{in} =380V, V_o =20V, 10% load.

CrCM ACF converter is designed and tested. The designed ACF prototype is shown in Fig.14, and the designed specification is same as simulation parameters in table I. Fig.15-16 show the voltage and current waveforms of CrCM ACF converter at different operating conditions, respectively. Fig.15 is the case when input voltage is 130V and 100% load. Fig.16 is the case when input voltage is 200V and 50% load. It is clearly seen that the ZVS status of the primary main power switch S_1 is fitly realized at the turn on instant by adopting the VF-PCM and discrete-ZVS control strategy. By comparing with the two operating conditions, because of the different input voltage and load current, the energy stored

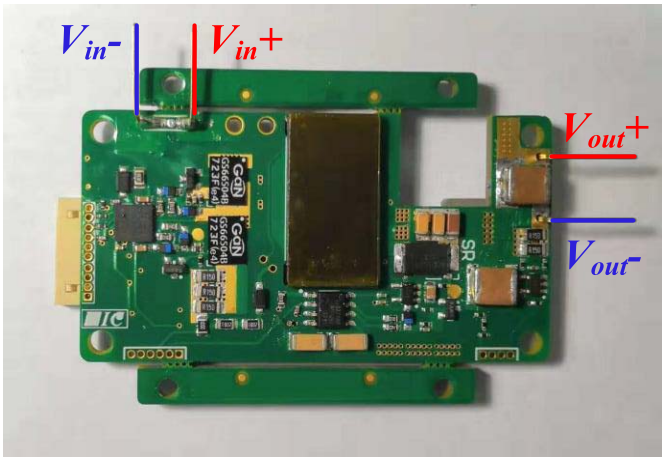

Fig. 14. Prototype of ACF converter.

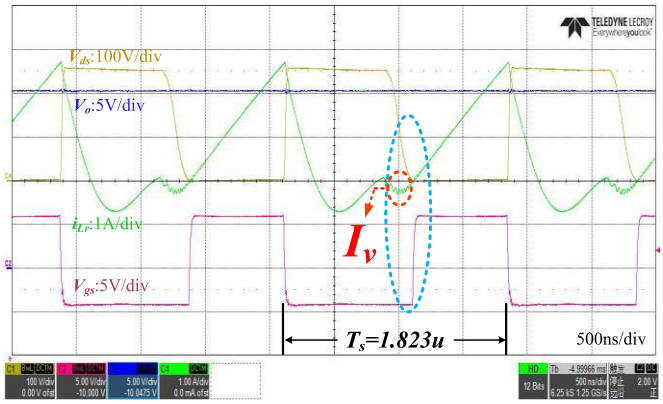

Fig. 15. The voltage and current waveforms when V_{in} =120V, 100% load.

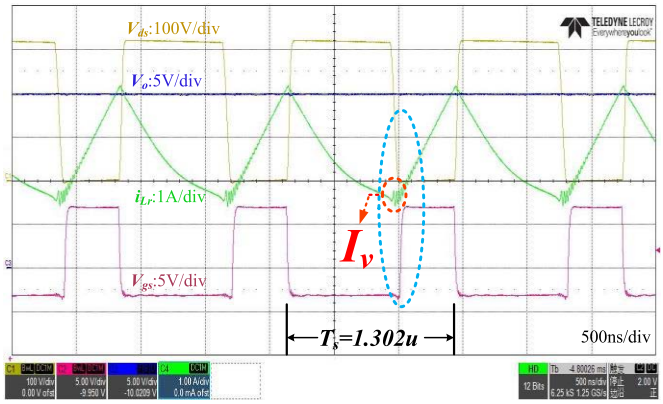

Fig. 16. The voltage and current waveforms when V_{in} =200V, 50% load.

in magnetizing inductor L_m which is used to realize ZVS of S_1 is different, then the needed valley current I_v and switching period T_s are also different.

The variation rule of magnetizing current valley I_v can be calculated by (36). According to this equation, in a constant switching frequency, Fig.17 given the relation among the needed negative current I_v, input voltage V_{in} and load current I_o. The absolute value of I_v increases as V_{in} increases and/or I_o decreases. Hence, when the switching frequency

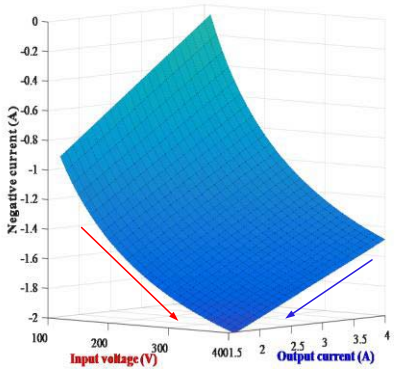

Fig. 17. The change rule of negative current I_v.

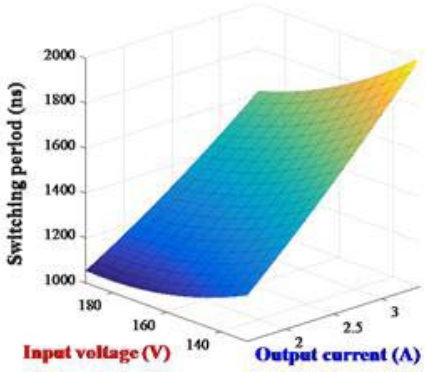

Fig. 18. The tested period on different status.

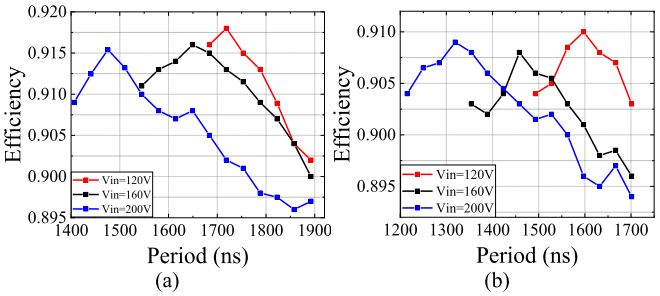

Fig. 19. The tested efficiency at different period and input voltage when (a) I_o = 3A and (b) I_o = 1.5A.

is fixed, the ZVS of S_1 may be realized with difficulty at low input voltage and high load, and the energy used to realize ZVS maybe redundant at high voltage and light load. Therefore, the need optimal switching period should be regulated for a proper ZVS realization, and which should be adjusted to increase as input voltage decreases and/or load current increases.

$$I_v = \frac{P_o}{V_{in}\eta} + \frac{I_o}{n} - \frac{1}{2L_m f_s}\frac{nV_oV_{in}}{nV_o + V_{in}} \tag{36}$$

By utilizing the proposed discrete-ZVS control method, the switching period is regulated and an appropriate negative magnetizing current is generated at every operating status, then the ZVS of S_1 problem is solved. Fig.18 presents the tested best switching period at different operating conditions by using

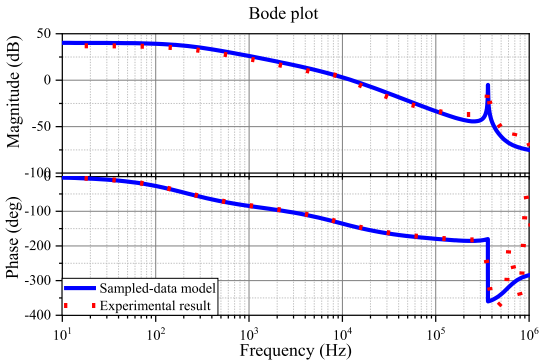

Fig. 20. Experimental verification G_{vc} when V_{in} =120V, 100% load.

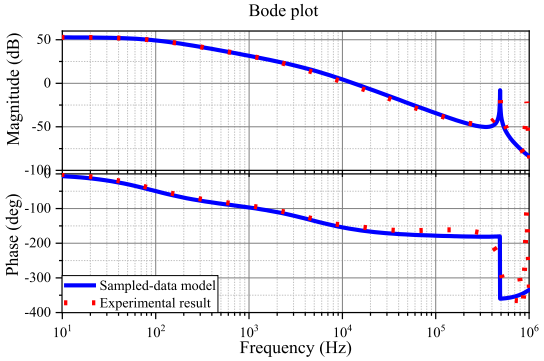

Fig. 21. Experimental verification G_{vc} when V_{in} =250V, 50% load.

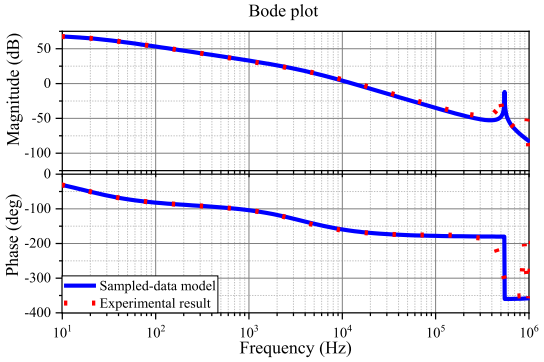

Fig. 22. Experimental verification G_{vc} when V_{in} =380V, 10% load.

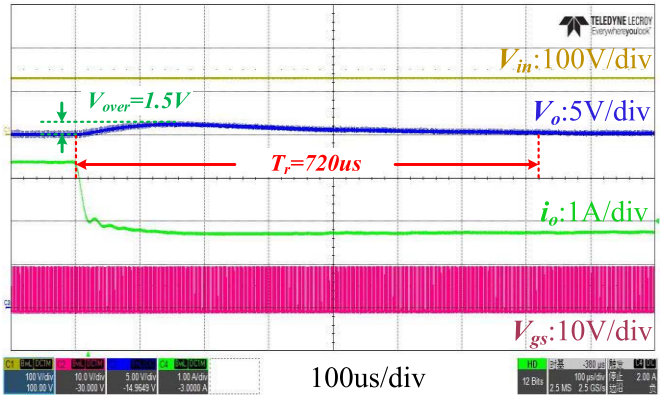

Fig. 23. Dynamic response from full-load to half-load at V_{in} = 130V.

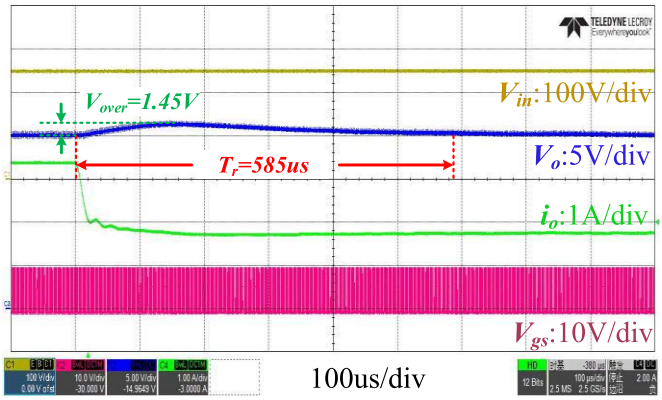

Fig. 24. Dynamic response from full-load to half-load at V_{in} = 250V.

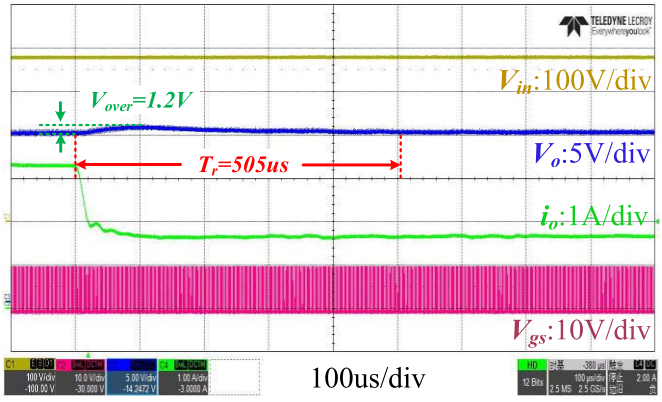

Fig. 25. Dynamic response from full-load to half-load at V_{in} = 380V.

discrete-ZVS control method. It can be seen that the switching period increases as input voltage decreases and/or load current increases.

Regulating switching period not only realize the ZVS of S_1, but also improve the operating efficiency. Fig.19 shows the tested efficiency at different input voltage and load current when switching period changes. It can be seen that the largest efficiency only can be obtained when ACF converter worked at the best period than another switching period. The power loss of power switch include turn-on loss and conduction loss during dead time T_{d2}. When the switching period T_s is smaller than the best T_s, the ZVS can not realized, so the turn-on loss will be increased. When the switching period T_s is larger than the best T_s, the flow current time across the body diode will be increased, and then the conduction loss will become large. Therefore, the best efficiency point only locate at the best switching period in a determined operating status.

Based on the designed CrCM ACF converter, the frequency responses at different work statuses are measured using network analyzer PSM1735, and the range of frequency measurements is conducted from 10Hz to 1MHz. In experiments, the working condition is selected as low input voltage high

load, middle input voltage middle load, and high input voltage light load, which are considered for representing the working range of the VF-PCM and discrete-ZVS controlled CrCM ACF converter. Fig.20-22 show the comparison of measured and calculated frequency characteristic curves of the control-to-output transfer function G_{vc} (s). It can be seen that the results of the proposed sampled-data model are in excellent agreement with the measurements in every frequency response test points.

Based on this CrCM ACF prototype and the proposed sampled-data model, the dynamic responses between different load statuses are measured. The compensating principle is followed by [38], [39]. Fig.23-25 show the dynamic responses when load steps from full-load to half-load, and the input voltage V_{in} is set at 130V, 250V, and 380V, respectively. In the three conditions, when the load current changed from full-load to half-load, the needed regulating time T_r is 720us, 585us, and 505us, respectively. The generated voltage overshoot V_{over} is 1.5V, 1.45V, and 1.2V, respectively. These parameters show good stability and transient responses for changes in load current, so which can satisfy the dynamic requirement in low power adaptor applications. Therefore, for engineering applications, the proposed sampled-data model can be well used in VF-PCM and discrete-ZVS controlled CrCM ACF converter.

VI. Conclusion

This paper proposes an accurate small signal model of VF-PCM and discrete-ZVS controlled CrCM ACF converter by using sampled-data modeling method. In the modeling process, the VF-PCM and discrete ZVS control process are all considered to obtain the complete frequency characteristic. The widely used control signal, duty ratio, in constant-frequency converter is replaced by the condition time of main power switch in CrCM ACF converter due to the variable-frequency switching characteristic. Through analysis, the total current close-loop transfer function can be deduced by the linear combination of the VF-PCM and discrete ZVS control model. Therefore, the VF-PCM and discrete-ZVS control model is established, respectively. After considering the sampling effect (H_{ep} and H_{ev}) and the modulator gain (F_{mp} and F_{mv}) of the two control models respectively, the control-to-output transfer function is developed. By comparing the proposed model with the single VF-PCM control model, Suntio's average model, and equivalent circuit model, it can be illustrated that the frequency characteristic has changed if the discrete-ZVS control method is adopted in CrCM ACF converter for high-efficiency. To verify the accuracy of the proposed sampled-data model, the SIMPLIS simulation and experimental results are also compared with. The comparison results show that the proposed model is basically agreement with the simulated and tested frequency response curve. In addition, the corresponding dynamic response from full-load to half-load express that the proposed sampled-data model can be well used in engineering applications.

References

[1] S.-H. Yang *et al.*, "High accuracy knee voltage detection for primary-side control in flyback battery charger," *IEEE Trans. Circuits Syst. I, Reg. Papers*, vol. 64, no. 4, pp. 1003–1012, Apr. 2017.

[2] F. Xie, R. Yang, and B. Zhang, "Bifurcation and border collision analysis of voltage-mode-controlled flyback converter based on total ampere-turns," *IEEE Trans. Circuits Syst. I, Reg. Papers*, vol. 58, no. 9, pp. 2269–2280, Sep. 2011.

[3] A. Ayachit, A. Reatti, and M. K. Kazimierczuk, "Magnetising inductance of multiple-output flyback DC–DC convertor for discontinuous-conduction mode," *IET Power Electron.*, vol. 10, no. 4, pp. 451–461, Mar. 2017.

[4] J. Zhang, H. Zeng, and X. Wu, "An adaptive blanking time control scheme for an audible noise-free quasi-resonant flyback converter," *IEEE Trans. Power Electron.*, vol. 26, no. 10, pp. 2735–2742, Oct. 2011.

[5] F.-C. Syu *et al.*, "Design and implementation of 1 MHz active-clamped resonant flyback converter," in *Proc. 43rd Annu. Conf. IEEE Ind. Electron. Soc. (IECON)*, Oct. 2017, pp. 4438–4442.

[6] T. LaBella, B. York, C. Hutchens, and J.-S. Lai, "Dead time optimization through loss analysis of an active-clamp flyback converter utilizing GaN devices," in *Proc. IEEE Energy Convers. Congr. Exposit. (ECCE)*, Sep. 2012, pp. 3882–3889.

[7] L. Xue and J. Zhang, "Active clamp flyback using GaN power IC for power adapter applications," in *Proc. IEEE Appl. Power Electron. Conf. Exposit. (APEC)*, Mar. 2017, pp. 2441–2448.

[8] Texas Instruments. *UCC28780: Adaptive Zero Voltage Switching Active-Clamp Flyback Controller*. [Online]. Available: http://www.ti.com/lit/ds/symlink/ucc28780.pdf

[9] On Semiconductor. *NCP1568: AC-DC active clamp flyback PWM IC*. [Online]. Available: https://www.onsemi.cn/pub/Collateral/NCP1568-D.PDF

[10] S. Amir, R. van der Zee, and B. Nauta, "An improved modeling and analysis technique for peak current-mode control-based boost converters," *IEEE Trans. Power Electron.*, vol. 30, no. 9, pp. 5309–5317, Sep. 2015.

[11] A. Luchetta, S. Manetti, M. C. Piccirilli, A. Reatti, and M. K. Kazimierczuk, "Comparison of DCM operated PWM DC-DC converter modelling methods including the effects of parasitic components on duty ratio constraint," in *Proc. IEEE 15th Int. Conf. Environ. Electr. Eng. (EEEIC)*, Jun. 2015, pp. 766–771.

[12] A. Davoudi, J. Jatskevich, and P. L. Chapman, "Averaged modelling of switched-inductor cells considering conduction losses in discontinuous mode," *IET Electr. Power Appl.*, vol. 1, no. 3, pp. 402–406, Jan. 2007.

[13] A. Luchetta, S. Manetti, M. C. Piccirilli, A. Reatti, and M. K. Kazimierczuk, "Effects of parasitic components on diode duty cycle and small-signal model of PWM DC-DC buck converter in DCM," in *Proc. IEEE 15th Int. Conf. Environ. Electr. Eng. (EEEIC)*, Jun. 2015, pp. 772–777.

[14] S.-Y. Chen, "Small-signal model for a flyback converter with peak current mode control," *IET Power Electron.*, vol. 7, no. 4, pp. 805–810, Apr. 2014.

[15] M. K. Kazimierczuk, *Pulse-Width Modulated DC-DC Power Converters*, 2nd. ed. Hoboken, NJ, USA: Wiley, 2015.

[16] A. Davoudi, J. Jatskevich, and P. L. Chapman, "Simple method of including conduction losses for average modelling of switched-inductor cells," *Electron. Lett.*, vol. 42, no. 21, pp. 1246–1267, 2006.

[17] M. Usman Iftikhar, P. Lefranc, D. Sadarnac, and C. Karimi, "Theoretical and experimental investigation of averaged modeling of non-ideal PWM DC-DC converters operating in DCM," in *Proc. IEEE Power Electron. Specialists Conf.*, Jun. 2008, pp. 2257–2263.

[18] M. Nashed and A. A. Fayed, "Current-mode hysteretic buck converter with spur-free control for variable switching noise mitigation," *IEEE Trans. Power Electron.*, vol. 33, no. 1, pp. 650–664, Jan. 2018.

[19] C.-F. Nien *et al.*, "A novel adaptive quasi-constant on-time current-mode buck converter," *IEEE Trans. Power Electron.*, vol. 32, no. 10, pp. 8124–8133, Oct. 2017.

[20] A. Luchetta, S. Manetti, M. C. Piccirilli, A. Reatti, and M. K. Kazimierczuk, "Derivation of network functions for PWM DC-DC buck converter in DCM including effects of parasitic components on diode duty-cycle," in *Proc. IEEE 15th Int. Conf. Environ. Electr. Eng. (EEEIC)*, Jun. 2015, pp. 778–783.

[21] A. Davoudi, J. Jatskevich, and T. D. Rybel, "Numerical state-space average-value modeling of PWM DC-DC converters operating in DCM and CCM," *IEEE Trans. Power Electron.*, vol. 21, no. 4, pp. 1003–1012, Jul. 2006.

[22] A. Davoudi, J. Jatskevich, and P. L. Chapman, "Numerical dynamic characterization of peak current-mode-controlled DC–DC converters," *IEEE Trans. Circuits Syst. II, Exp. Briefs*, vol. 56, no. 12, pp. 906–910, Dec. 2009.

[23] B. Bryant and M. K. Kazimierczuk, "Voltage loop of boost PWM DC-DC converters with peak current-mode control," *IEEE Trans. Circuits Syst. I, Reg. Papers*, vol. 53, no. 1, pp. 99–105, Jan. 2006.

[24] A. Reatti and M. Balzani, "Computer aided small-signal analysis for PWM DC-DC converters operated in discontinuous conduction mode," in *Proc. 48th Midwest Symp. Circuits Syst.*, Aug. 2005, pp. 1561–1564.

[25] G. N. Love and A. R. Wood, "Small signal model of a power electronic converter," in *Proc. IEEE IPEC*, Dec. 2007, pp. 636–642.

[26] A. Reatti and M. Balzani, "PWM switch model of a buck-boost converter operated under discontinuous conduction mode," in *Proc. 48th Midwest Symp. Circuits Syst.*, Aug. 2005, pp. 667–670.

[27] A. Ayachit, A. Reatti, and M. K. Kazimierczuk, "Small-signal modeling of PWM dual-SEPIC DC-DC converter by circuit averaging technique," in *Proc. 42nd Annu. Conf. IEEE Ind. Electron. Soc. (IECON)*, Oct. 2016, pp. 3606–3611.

[28] T. Suntio, "Average and small-signal modeling of self-oscillating flyback converter with applied switching delay," *IEEE Trans. Power Electron.*, vol. 21, no. 2, pp. 479–486, Mar. 2006.

[29] J. H. Park and B. H. Cho, "Small signal modeling of hysteretic current mode control using the PWM switch model," in *Proc. IEEE Workshops Comput. Power Electron.*, Jul. 2006, pp. 225–230.

[30] A. Ayachit, A. Reatti, and M. K. Kazimierczuk, "Small-signal modeling of the PWM boost DC-DC converter at boundary-conduction mode by circuit averaging technique," in *Proc. IEEE Int. Symp. Circuits Syst. (ISCAS)*, May 2015, pp. 229–232.

[31] B. Bryant and M. K. Kazimierczuk, "Modeling the closed-current loop of PWM boost DC-DC converters operating in CCM with peak current-mode control," *IEEE Trans. Circuits Syst. I, Reg. Papers*, vol. 52, no. 11, pp. 2404–2412, Nov. 2005.

[32] R. Pagano, "Sampled-data modeling of hysteretic converters accounting for intracycle waveform propagation," *IEEE Trans. Circuits Syst. I, Reg. Papers*, vol. 58, no. 3, pp. 619–632, Mar. 2011.

[33] C.-H. Cheng, C.-J. Chen, and S.-S. Wang, "Small-signal model of flyback converter in continuous-conduction mode with peak-current control at variable switching frequency," *IEEE Trans. Power Electron.*, vol. 33, no. 5, pp. 4145–4156, May 2018.

[34] P.-H. Liu, "Design consideration of active clamp flyback converter with highly nonlinear junction capacitance," in *Proc. IEEE Appl. Power Electron. Conf. Exposit. (APEC)*, Mar. 2018, pp. 783–790.

[35] J. Park, J. Fan, X. Wang, and A. Huang, "A sample-data model for double edge current programmed mode control (DECPM) in high-frequency and wide-range DC–DC converters," *IEEE Trans. Power Electron.*, vol. 25, no. 4, pp. 1023–1033, Apr. 2010.

[36] S. Xu, F. Li, Y. Yao, S. Lu, and W. Sun, "A high-frequency model for a PCM buck converter," *IEEE Trans. Power Electron.*, vol. 30, no. 4, pp. 2304–2312, Apr. 2015.

[37] H. Li, J. Shang, B. Zhang, X. Zhao, N. Tan, and C. Liu, "Stability analysis with considering the transition interval for PWM DC-DC converters based on describing function method," *IEEE Access*, vol. 6, pp. 48113–48124, 2018.

[38] K. Heong Ang, G. Chong, and Y. Li, "PID control system analysis, design, and technology," *IEEE Trans. Control Syst. Technol.*, vol. 13, no. 4, pp. 559–576, Jul. 2005.

[39] F. Salinas, M. Ghanes, J. P. Barbot, M. F. Escalante, and B. Amghar, "Modeling and control design based on Petri nets for serial multicellular choppers," *IEEE Trans. Control Syst. Technol.*, vol. 23, no. 1, pp. 91–100, Jan. 2015.

Shengyou Xu was born in Henan, China, in 1993. He received the B.S. degree in measurement and control technology and instrumentation from Liaoning Technical University, Huludao, China, in 2016. He is currently pursuing the Ph.D. degree in electronics engineering from Southeast University, Nanjing, China.

His current research interests include modeling and control technology of high-frequency power conversion.

Qinsong Qian received the Ph.D. degree in electronics engineering from Southeast University, Nanjing, China, in 2012.

In 2012, he joined the School of Electronic Science and Engineering, Southeast University, where he is currently an Associate Professor. His current research interests include power converter design, simulations, and reliability.

Ran Shi received the B.S. degree in microelectronics science and engineering from the Hefei University of Technology, China, in 2017. She is currently pursuing the master's degree in microelectronics and solid-state electronics with Southeast University, Nanjing, China.

Her current research interests include high-frequency electromagnetic and transformer.

Syed Sikandar Shah received the B.S degree in electronics engineering from the Balochistan University of Information Technology, Engineering and Management Sciences, in 2013. He is currently pursuing the Ph.D. with Southeast University, Nanjing, China.

Qi Liu was born in Jiangsu, China, in 1993. He received the B.S. degree in electronics engineering from Yangzhou University, Yangzhou, China, in 2015. He is currently pursuing the Ph.D. degree in electronics engineering with Southeast University, Nanjing, China.

His current research interests include the digital control strategy for high-frequency and high-efficiency power conversion.

Shengli Lu received the Ph.D. degree in information and physics from Nanjing University, Nanjing, China, in 1994.

His current research interests include VLSI and application-specific integrated circuit.

Weifeng Sun (Senior Member, IEEE) received the B.S., M.S., and Ph.D. degrees in electronic engineering from Southeast University, Nanjing, China, in 2000, 2003, and 2007, respectively.

Since 2006, he has been with the School of Electronic Science and Engineering, Southeast University, where he is currently a Professor. His research interests include new power device design, power ICs, power device modeling, and power systems.